PCCP

Phase Behaviour and Conductivity of Supporting Electrolytes in Supercritical Difluoromethane and 1,1-Difluoroethane

Journal:	*Physical Chemistry Chemical Physics*
Manuscript ID	CP-ART-01-2016-000466.R1
Article Type:	Paper
Date Submitted by the Author:	30-Mar-2016

Complete List of Authors:	Han, Xue; University of Nottingham, School of Chemistry Ke, Jie; University of Nottingham, School of Chemistry Norhidayah, Suleiman; University of Nottingham, School of Chemistry Levason, W; University of Southampton, School of Chemistry Pugh, David; University of Southampton, School of Chemistry Zhang, Wenjian; University of Southampton, School of Chemistry Reid, Gillian; University of Southampton, School of Chemistry Licence, Peter; The University of Nottingham, School of Chemistry George, Michael W; University of Nottingham, School of Chemistry

Phase Behaviour and Conductivity of Supporting Electrolytes in Supercritical Difluoromethane and 1,1-Difluoroethane

Xue Han,[a] Jie Ke,[a] Norhidayah Suleiman,[a] William Levason,[b] David Pugh,[b] Wenjian Zhang,[b] Gillian Reid,[b] Peter Licence,[a] Michael W. George *[a,c]

[a] School of Chemistry, University of Nottingham, University Park, Nottingham NG7 2RD, UK.

[b] School of Chemistry, University of Southampton, Highfield, Southampton, SO17 1BJ, UK.

[c] Department of Chemical and Environmental Engineering, University of Nottingham Ningbo China, 199 Talking East Road, Ningbo 315100, China.

* Corresponding author's E-mail: mike.george@nottingham.ac.uk

Abstract

We present investigations into a variety of supporting electrolytes and supercritical fluids probing the phase and conductivity behaviour of these systems and show that they not only provide sufficient electrical conductivity for an electrodeposition bath, but match the requirements imposed by the different precursors and process parameters e.g. increased temperature for potential deposition experiments. The two supercritical fluids that have been explored in this study are difluoromethane (CH_2F_2) and 1,1-difluoroethane (CHF_2CH_3). For CH_2F_2, the phase behaviour and electrical conductivity of eight ionic compounds have been studied. Each compound consists of a cation and an anion from the selected candidates (i.e. tetramethylammonium ($[N(CH_3)_4]^+$), tetrabutylammonium ($[N(^nC_4H_9)_4]^+$), 1-ethyl-3-methylimidazolium ($[EMIM]^+$) and 1-butyl-3-methylimidazolium ($[BMIM]^+$) for cations, and **t**etrakis-*n*butylammonium tetrakis(perfluoro-tert-butoxy)aluminate ($[Al(OC(CF_3)_3)_4]^-$), chloride (Cl^-), trifluoromethyl sulfonimide ($[NTf_2]^-$) and tris(pentafluoroethyl)trifluorophosphate ($[FAP]^-$) for anions). For CHF_2CH_3, $[N(^nC_4H_9)_4][BF_4]$ and $[N(^nC_4H_9)_4][B\{3,5\text{-}C_6H_3(CF_3)_2\}_4]$ have been investigated for comparison with the previously measured solubility and conductivity in CH_2F_2.

We have found that $[N(^nC_4H_9)_4][Al(OC(CF_3)_3)_4]$, $[N(^nC_4H_9)_4][FAP]$ and $[N(CH_3)_4][FAP]$ have much higher molar conductivity in $scCH_2F_2$ at similar conditions than $[N(^nC_4H_9)_4][BF_4]$, a widely used commercial electrolyte. Additionally, $scCHF_2CH_3$ shows potential for use as the solvent for SCFED, especially at high temperatures since high density of this fluid can be achieved at lower operating pressures than similar fluids that can be used to produce electrochemical baths with comparable conductivity.

Keywords: supercritical fluid; phase equilibrium; conductivity; difluoromethane; 1,1-difluoroethane; supporting electrolytes

1 Introduction

Supercritical Fluid Electrodeposition (SCFED) is a relatively new development in the area of electrodeposition and this approach exploits some of the advantages of supercritical fluids (SCFs), such as the lack of surface tension, which enables them to penetrate to the bottom of nano-pores with enhanced mass transport rates.[1, 2] The successful electrodeposition of Cu, Ag, Ge and other metals and semiconductors [3-7] on flat substrates and the production of 3 nm Cu wires in silica templates[8] either from supercritical CO_2/CH_3CN mixtures or from supercritical hydrofluorocarbons (HFCs) has recently been demonstrated. Electrodeposition from SCFs requires appropriately designed precursors and a carefully chosen supporting electrolyte that is sufficiently soluble and dissociated in the SCF. The high conductivity is particularly important for the electrodeposition process because of the need to pass large currents. The phase of the multicomponent fluid in the electrodeposition bath also greatly affects the process and particularly the quality of the final deposit. For example, the operation in 2-phase conditions may thwart the unique properties of supercritical fluids we are trying to utilise. Under other conditions the generation of gas bubbles on the surface of substrates is undesirable, and may be suppressed under supercritical conditions. Therefore, the investigation of the properties of the SCFED bath can provide key information on the selection of the deposition conditions and help to establish the relationship between the quality of films/devices and the operating conditions.

The fundamental electrochemical investigations of electrolytes in SCFs have been carried out by several research groups. For example, Wightman and co-workers[9] performed cyclic voltammetry studies in supercritical carbon dioxide ($scCO_2$) using tetrahexylammonium hexafluorophosphate ($[N(^nC_6H_{13})_4][PF_6]$) as the supporting electrolyte. The double layer capacitance and the conductivity of long chain quaternary ammonium electrolytes in $scCO_2$ was also studied by Abbott and Harper.[10, 11]

Beyond CO_2, supercritical HFCs have also been used as solvents for electrochemistry studies due to their wider electrochemical potential windows.[12] The dielectric constants of some commonly used HFCs, such as difluoromethane (CH_2F_2), 1,1,1,2-tetrafluoroethane (CH_2FCF_3) and 1,1-difluoroethane (CH_3CHF_2) has been measured by several research groups.[11, 13, 14] Olsen and Tallman[15, 16] also measured the diffusion coefficients of ferrocene and cobaltocenium hexafluorophosphate in chlorodifluoromethane ($CHClF_2$) using tetrabutylammonium tetrafluoroborate ($[N(^nC_4H_9)_4][BF_4]$) as the supporting electrolyte. The conductivity of $[N(^nC_4H_9)_4][BF_4]$ in liquid and supercritical CH_2FCF_3 and CH_2F_2 as a function of pressure and concentration was investigated by Abbott and Eardly,[17] showing that sufficient conductivity can be obtained to allow electrochemical studies.

We have also reported a range of non-aqueous electrolyte systems, which also provide sufficient electrical conductivity for carrying out electrodeposition in SCFs. Our experimental studies demonstrated that three approaches can be adopted to increase the solubility/conductivity of ionic compounds in SCFs: (i) using polar co-solvents with CO_2; (ii) using HFCs with relativity high dielectric constants (e.g. CH_2F_2 and CHF_3); and (iii) using bulky fluorinated cations and/or anions.[18] In particular, we have shown that, although CH_3CN ($\varepsilon = 37$) and CH_3OH ($\varepsilon = 33$) have a similar dielectric constant, CH_3CN is a more effective co-solvent than CH_3OH, based on the phase equilibrium data from the ternary system of CO_2 + $[N(^nC_4H_9)_4][BF_4]$ + co-solvent.[19] The benchmark compound $[N(^nC_4H_9)_4][B\{3,5\text{-}C_6H_3(CF_3)_2\}_4]$, was used to show that the CH_2F_2 system has a molar conductivity 3–8 times higher than the CO_2 + CH_3CN system (x_{CH3CN}/x_{CO2} = ~0.12) at the same concentration of the electrolyte in the near- or super-critical conditions.[20] In these studies, understanding the phase behaviour is required for a full understanding of the system. Furthermore, among the three approaches listed above, finding appropriate cations, anions and their combinations is of highest importance to obtain high solubility and conductivity in low-polarity SCFs, not only because the solubility and conductivity are strongly affected by the size of the cations/anions and their interactions with each other and with solvent molecules, but because a successful supporting electrolyte must be compatible with the reagents and additives used in a specific SCFED process. We have previously evaluated a series of supporting electrolytes containing four types of cations (Na^+, $[N(^nC_4H_9)_4]^+$, $[NR_f(CH_3)_3]^+$, $[NR_f(^nC_4H_9)_3]^+$, $R_f = CF_3(CF_2)_7(CH_2)_3$ and five types of anions ($[BF_4]^-$, $[B(C_6F_5)_4]^-$, $[B(C_6H_4F)_4]^-$, $[B(4\text{-}C_6H_4CF_3)_4]^-$ and $[B\{3,5\text{-}C_6H_3(CF_3)_2\}_4]^-$).[19, 20] The compounds with the $[B\{3,5\text{-}C_6H_3(CF_3)_2\}_4]^-$ anion show the highest conductivities in both CO_2/CH_3CN and CH_2F_2, suggesting that bulky fluorinated anions do improve the conductivity of the supporting electrolytes in SCFs through promoting ion dissociation and triplet-ion formation. In terms of selecting cations, the electrolyte of Na^+ with $[B\{3,5\text{-}C_6H_3(CF_3)_2\}_4]^-$, surprisingly, gives much higher conductivity (2.55×10^{-2} S m^2 mol^{-1}) than its $[N(^nC_4H_9)_4]^+$ analogue (1.97×10^{-2} S m^2 mol^{-1}) in scCH_2F_2.[20] Moreover, there is

no significant improvement of the conductivity in either CO_2/CH_3CN or CH_2F_2 when using the ammonium cation bearing a long fluorinated alkyl chain.

Temperature is another key parameter to control the quality of the films/devices manufactured by using electrodeposition methods. Recent reports have used $scCF_2H_2$ and in order to access higher temperatures with similar density higher operating pressures will be necessary. This is an important consideration for the SCFED processes across a wide range of temperatures as the solubility and electrical conductivity of the supporting electrolytes in SCFs may be expected to decrease considerably with increasing temperature at a given pressure. The temperature-pressure-density relationship of a fluid in the near-critical region suggests that if the electrodeposition temperature is near the critical temperature (T_c) of the fluid, the fluid density can be maintained close to, or above, its critical density without applying a very high pressure (e.g. > 50 MPa). Therefore, an SCF with high T_c is expected to be preferential when carrying out SCFED at high temperatures.

In this paper, we have investigated two SCFs for SCFED. The first, CH_2F_2, has been previously shown to be suitable for SCFED due to its high dipole moment (μ = 1.98 D [21]) and moderate T_c (351.26 K)[22]. We explore the use of a series of supporting electrolytes which are chemically stable at high-temperatures, easy to synthesise with high purity, and compatible with halometallate precursors such as those used for electrodeposition of germanium[4] and a range of other p-block elements[23]. For such systems, experimental studies on the phase equilibrium of the CH_2F_2 mixtures with the supporting electrolytes consisting of the anions (such as fluorinated aluminate, chloride, trifluoromethyl sulfonimide and tris(pentafluoroethyl) trifluorophosphate) must first be understood before probing the conductivity behaviour. In addition to the quaternary ammonium cations studied, we have also investigated two imidazolium cations, which are common cations in ionic liquids used for electroplating.[24]

The second SCF selected is 1,1-difluoroethane (CHF_2CH_3), which has a critical temperature and critical pressure (p_c) of 386.4 K and 4.52 MPa[22], respectively. It has a high dipole moment (2.27 D)[21] and dielectric constant (ε_r = 7 at 363.15K and 2.9 MPa) [25] among the HFCs, making it a potential supercritical fluid for dissolving ionic species and carrying out electrodeposition.[26] In order to compare the phase and conductivity behaviours with those in CH_2F_2, the two well-characterised supporting electrolytes ($[N(^nC_4H_9)_4][BF_4]$ and $[N(^nC_4H_9)_4][B\{3,5\text{-}C_6H_3(CF_3)_2\}_4]$) were chosen and the measurements made at 393.15 K, i.e. 7 K and 42 K, respectively, above the T_c of CHF_2CH_3 and CH_2F_2.

2 Experimental

2.1 Chemicals

Difluoromethane (Apollo Scientific, 99.9 wt/wt%) and 1,1-difluoroethane (BOC, 99.5% wt/wt%) were used as supplied. Tetrabutylammonium chloride ($[N(^nC_4H_9)_4]Cl$) (Fluka, puriss,, ≥99.0%) and Tetrabutylammonium tetrafluoroborate ($[N(^nC_4H_9)_4][BF_4]$) (Fluka, electrochemical grade, ≥99.0%) were used without further purification. The other eight imidazole and quaternary ammonium based ionic compounds were synthesised under anhydrous conditions and stored in an argon-purged glovebox prior to use. The chemical structures of the compounds studied in this paper are listed in Table 1. The preparation and characterisation of $[N(CH_3)_4][FAP]$ ($[FAP]^- = [PF_3(C_2F_5)_3]^-$), $[N(^nC_4H_9)_4][FAP]$ and $[N(^nC_4H_9)_4][Al(OC(CF_3)_3)_4]$ are given in detail in the supplementary information.

2.2 High-pressure apparatus and measurement procedures

The phase equilibrium of the binary systems with the HFC (CH_2F_2 or CHF_2CH_3) was studied by using a variable-volume view cell, the detailed description of which can be found in the literature.[27] Since most of the supporting electrolytes used in this study are hygroscopic, they were handled in a glovebox and transferred to the view-cell in an argon-purged sealed glass vial. The experimental procedures are briefly described as follows. The equilibrium vessel was first purged with argon three times, and then loaded with the supporting electrolyte. The mass of the ionic compounds was determined by using an analytical balance (Mettler Toledo, AL204) placed in the glovebox. The HFC was introduced into the view-cell from a high-pressure sample cylinder (Swagelok, 316L-50DF4-150). The mass difference of the sample cylinder was used to obtain the amount of HFC which had been added. For each mixture with a given composition (e.g. the mole fraction of the ionic compound), the *p-T* phase boundary was determined by the observation of the phase transition at a series of temperatures between 293 K and 398 K. The relative standard uncertainty of the mole fraction for the supporting electrolytes (x_1) in the mixtures is ~1% (e.g. the standard uncertainty $u(x_1) = 0.00004$ when $x_1 = 0.00400$). The estimated standard uncertainty is 0.2 K for the temperature measurements and 0.04 MPa for the pressure measurements. The combined standard uncertainty was estimated as 0.1 MPa for the phase transition pressures reported in this work.

The electrical conductivity of the CH_2F_2 mixtures was measured using a newly purpose-built conductivity apparatus. The schematic diagram of the apparatus is shown in Figure 1. The conductivity vessel is made from stainless steel, consisting of three pieces, i.e. a main body (MB), a hollow screw (HS) and an electrode holder (EH). The electrode holder is sealed to the main body

with a PTFE seal (SE). Two pieces of platinum foil (0.5 cm^2 each) are mounted to the inner surface of a glass tube that is attached to the electrode holder. The platinum connection wires for the platinum electrodes are embedded in the PEEK (polyetheretherketone) tubing and epoxy resins. The PEEK tubing is fed through the electrode holder and the hollow screw and is sealed to the holder by the SSI 1/16 inch fittings.

Both the conductivity vessel and the preheater (PH) are immersed in an oil bath (Julabo, model F32) with the temperature stability better than 0.05 K. The temperature of the sample was measured by a platinum resistive thermal device (RTD, RS Components, Pt100), calibrated against a standard platinum RTD probe. The uncertainty of the temperature measurements was estimated to be less than 0.1 K for all of our conductivity measurements. The conductivity vessel was connected to the fluid delivery unit using PEEK tubing to avoid possible current leakage to the ground. The system pressure was measured by the pressure transducer (supplied by RDP Electronics Ltd, Super-TJE, 0–34.5 MPa) with an accuracy of ±0.017 MPa (±2.5 psi). The maximum working temperature and pressure of the conductivity apparatus is 400 K and 27 MPa, respectively.

Initially a known amount of the supporting electrolyte was placed at the bottom of the conductivity vessel, which was sealed and evacuated for 30 minutes. The vessel was filled with ~ 0.5 MPa of the HFC and then it was placed into the oil bath and heated to the desired temperature (e.g. 363 K). After the system temperature reached the desired temperature, the pressure of the system was increased stepwise by pumping CH_2F_2 into the vessel. At each pressure step the contents in the vessel were agitated for more than 10 minutes before the conductivity was recorded. During the conductivity measurements valve V2 (Figure 1) was closed to isolate the conductivity vessel and the pump, and the stirrer was switched off. Since no supporting electrolyte had been withdrawn from the vessel during the measurements, the molar concentration of the ionic compound was kept constant during a series of measurements at 10-13 different pressures. The conductivity measurements were made with a JENWAY 4520 conductivity meter. The cell constant was calibrated using the conductivity solutions of KCl after platinisation of the platinum electrodes using the standard procedures.[28] The estimated relative uncertainty is ~ ±1% in the conductivity measurements. The mass of the ionic compound was measured by using an analytical balance (Mettler Toledo AB256-S) with the readability, repeatability and linearity (fine range) of 0.01 mg, 0.03 mg and 0.2 mg, respectively. The volume of the conductivity vessel (9.95±0.01 cm^3, with the magnetic stirrer and the electrodes in place) was determined by using the gas expansion method.

3 Results and discussion

3.1 Phase behaviour

3.1.1 Phase behaviour of eight supporting electrolytes in CH_2F_2. We have examined the solubility of the compounds with 4 different anions (i.e. Cl^-, $[NTf_2]^-$, $[FAP]^-$, $[Al(OC(CF_3)_3)_4]^-$, see Table 1) in CH_2F_2. All of these anions are either commercially available or relatively easily synthesised and purified. $[Al(OC(CF_3)_3)_4]^-$ is a potential candidate for high-temperature SCFED processes based upon comparative data on the stability of the Al-O bonds *vs*. the B-C bonds in $[B\{(3,5\text{-}CF_3)_2C_6H_3\}_4]^-$. In addition to the two quaternary ammonium cations ($[N(^nC_4H_9)_4]^+$ and $[N(CH_3)_4]^+$), we have also included two imidazolium-based cations ($[BMIM]^+$ and $[EMIM]^+$). Table 1 lists 8 ionic compounds selected from combinations of the above 4 cations and 4 anions.

The phase equilibrium of the binary mixtures with CH_2F_2 and the electrolytes was measured by using a so-called synthetic approach[29] in the variable-volume view-cell. The phase diagrams are presented in the p, T-space for the mixture with a given composition. Typical p-T phase diagrams are depicted in Figure 2 using the binary system of $[EMIM][NTf_2]$ + CH_2F_2 as an example. The region above the phase boundary is the single-phase region, which is the preferential condition for the electrodeposition in SCFs.

$[EMIM][NTf_2]$ is a viscous liquid at ambient conditions. After liquid CH_2F_2 was condensed into the view-cell, $[EMIM][NTf_2]$ is completely miscible with the CH_2F_2, resulting in only two phases (a gaseous CH_2F_2 phase on the top and a liquid phase at the bottom) co-existing in the cell. Our measured temperature range covers both the sub- and super-critical states (290-370 K). As can be seen from Figure 2, the pressure needed to reach the one-phase region increases with rising temperature for all of the 5 mixtures with different compositions between 1.9×10^{-4} and 4.25×10^{-3} (mole fraction). When the temperature is below the T_c of CH_2F_2 (351 K), the phase transition pressures are only slightly different from each other for the mixtures with different compositions. The phase boundaries at these conditions ($T < T_c$) represent the equilibrium between a vapour phase with virtually no $[EMIM][NTf_2]$ and a liquid phase with dissolved $[EMIM][NTf_2]$. The vapour pressure of the liquid CH_2F_2 phase is not changed significantly because the mole fraction of $[EMIM][NTf_2]$ in the liquid phase is low. When the temperature approaches T_c, the nature of the phase transition switches from the liquid-vapour to the liquid-fluid transition. The one-phase region can be reached when all the electrolyte is dissolved into the dense fluid-phase to form a homogeneous solution. Because CH_2F_2 is highly compressible in the supercritical region, higher pressures are required to increase the fluid density to achieve higher solubility of $[EMIM][NTf_2]$ in the CH_2F_2 phase. This is illustrated by the phase boundary shifting up to higher pressures for more concentrated mixtures.

To compare the effects of cations/anions on the solubility of electrolytes in CH_2F_2, we have measured the p-T phase boundaries of the 8 binary mixtures containing a similar mole fraction of electrolyte (i.e. $x = \sim 5\times10^{-4}$) between 290 and 370 K, see Figure 3. For all 8 of the isopleths the phase transition pressure increases with temperature, resembling the phase diagrams shown in Figure 2.

Figure 3a shows the p-T phase boundary of 4 ionic compounds with the same cation ($[N(^nC_4H_9)_4]^+$) but 4 different anions (i.e. Cl^-, $[NTf_2]^-$, $[FAP]^-$, $[Al(OC(CF_3)_3)_4]^-$). Between 290 and 350 K, the phase boundaries of these binary mixtures are almost superimposed, while the phase boundaries start to diverge when the temperature is above 350 K. One can see that although all of the phase transition pressures are below 10 MPa at 363.15 K for the 4 tetrabutylammonium electrolytes, the electrolyte with $[NTf_2]^-$ requires the lowest pressure, then followed by Cl^-, $[FAP]^-$, $[Al(OC(CF_3)_3)_4]^-$.

When using $[EMIM]^+$ as the cation, the Cl^- and the $[NTf_2]^-$ electrolytes behave very differently from the $[N(^nC_4H_9)_4]^+$ electrolytes when T > 340 K. The phase transition pressure is 1.6 MPa higher for [EMIM]Cl than for $[EMIM][NTf_2]$ at 363.15 K (Figure 3b). A separate test has been carried out for the [EMIM]Cl mixture at a higher concentration ($x_{[EMIM]Cl} = 1.1\times10^{-3}$), showing that [EMIM]Cl cannot completely dissolve in CH_2F_2 at 363.15 K even when the pressure is above 21 MPa

Examining the effects of the cations on the phase transition pressure, we can see that from Figure 3c for the three $[NTf_2]^-$ electrolytes, the phase transition pressure follows the order: $[BMIM]^+ < [N(^nC_4H_9)_4]^+ < [EMIM]^+$, suggesting that $[BMIM][NTf_2]$ has the highest solubility in CH_2F_2. For the two $[FAP]^-$ electrolytes, the length of alkyl chain (methyl *vs.* butyl) on the ammonium cation has almost no effect on the phase transition pressures for the two mixtures shown in Figure 3d. Unlike the two highly fluorinated anions ($[NTf_2]^-$ and $[FAP]^-$), the choice of cations is crucial for increasing the solubility of the chloride electrolytes in $scCH_2F_2$. Figure 3e shows that the phase transition pressure at 363.15 K is 2.2 MPa higher for [EMIM]Cl than for $[N(^nC_4H_9)_4]Cl$, even for a very dilute solution ($x = \sim 5\times10^{-4}$). It is worth noting that among the 4 anions studied in this work and the other anions reported previously,[19, 20] Cl^- is the only anion without any fluorinated functional groups and its ionic radius is much smaller than the fluorinated tetra-arylborate anions ($[BAr^F]^-$), making it an attractive candidate for SCFED in extreme nano-pores.

For the 8 binary mixtures measured in CH_2F_2, the phase diagram of $[N(^nC_4H_9)_4][Al(OC(CF_3)_3)_4] + CH_2F_2$ differs from all the others by showing very similar phase boundaries over the entire temperature range (290-370 K) with the mole fraction of $[N(^nC_4H_9)_4][Al(OC(CF_3)_3)_4]$ from 4.3×10^{-4} to 5.27×10^{-3} (Figure 4b). A closer look at the data reveals that at low temperatures (T < 310 K), the

transition pressure required to reach a one-phase region decreases marginally with increasing the $[N(^nC_4H_9)_4][Al(OC(CF_3)_3)_4]$ mole fraction. The difference in transition pressure between the 5 binary systems with different mole fraction becomes smaller and eventually negligible when the temperature approaches 350 K. Above 350 K, the mole fraction dependence of the transition pressure is reversed, showing that with higher $[N(^nC_4H_9)_4][Al(OC(CF_3)_3)_4]$ mole fraction, higher pressure is needed to reach a one-phase region (e.g. at 363.15 K).

By interpolating the data shown in Figure 4b, the p–x phase diagram of the binary system of $[N(^nC_4H_9)_4][Al(OC(CF_3)_3)_4] + CH_2F_2$ can be obtained at 363.15 K, as depicted in Figure 4a, together with the the p–x diagrams for the other binary systems ($[N(^nC_4H_9)_4]Cl + CH_2F_2$ and $[EMIM][NTf_2] + CH_2F_2$). As can be seen from the figure, the solubility of $[N(^nC_4H_9)_4][Al(OC(CF_3)_3)_4]$ is less pressure dependent than that of $[N(^nC_4H_9)_4]Cl$ and $[EMIM][NTf_2]$ in CH_2F_2. For example, the increase in phase-transition pressure for $[N(^nC_4H_9)_4][Al(OC(CF_3)_3)_4] + CH_2F_2$ is only ~0.5 MPa at 363.15 K when the mole fraction of the electrolytes increases from 4.3×10^{-4} to 5.3×10^{-3}, whereas the increase in the transition pressure for the other two systems is >1.5 MPa. Thus within the studied concentration range no higher pressure is required to form a homogeneous fluid phase for the system with high mole fraction of $[N(^nC_4H_9)_4][Al(OC(CF_3)_3)_4]$.

3.1.2 Phase behaviour of $[N(^nC_4H_9)_4][BF_4]$ and $[N(^nC_4H_9)_4][B\{(3,5\text{-}CF_3)_2C_6H_3\}_4]$ in CHF_2CH_3. For the phase equilibrium measurements of the CHF_2CH_3 systems, we first extended our previous work[20] and examined $[N(^nC_4H_9)_4][BF_4]$ as the supporting electrolyte in the temperature between 293 K and 398 K and at pressures up to 20 MPa. The p-T phase diagrams are depicted in Figure 5a for the four binary mixtures with $x_{[N(^nC_4H_9)_4][BF_4]}$ ranging from 1.67×10^{-3} to 1.58×10^{-2}. The corresponding phase equilibrium data are listed in Table S3 in the supplementary information. Similar to the phase behaviour of the $[N(^nC_4H_9)_4][BF_4] + CH_2F_2$ system, the phase-transition pressure increases with increasing temperature for a mixture with a given composition. Figure 5a and Table S4 in the supplementary information also present new data of the p-T phase boundary for the $[N(^nC_4H_9)_4][BF_4] + CH_2F_2$ mixture with $x_{[N(^nC_4H_9)_4][BF_4]} = 4.17\times10^{-3}$, measured at temperatures up to 398 K. As can be seen from the figure, the phase-transition pressure for the mixture with the same $x_{[N(^nC_4H_9)_4][BF_4]}$ (~4.2×10^{-3}) decreases considerably from 15.7 MPa for the CH_2F_2 system to 7.8 MPa for the CHF_2CH_3 system at 393.15 K. The p-*x* phase diagram (Figure 5b) shows clearly that at 393.15 K $[N(^nC_4H_9)_4][BF_4]$ is much more soluble in CHF_2CH_3 than in CH_2F_2 over a wide composition range.

Further phase behaviour measurements were carried out with $[N(^nC_4H_9)_4][B\{(3,5\text{-}CF_3)_2C_6H_3\}_4]$, which had been proven previously to give high solubility and conductivity in CH_2F_2.[20] Figure 6 shows that this salt also has high solubility in CHF_2CH_3. For example, when the binary mixture

contains 1.7×10^{-3} (mole fraction) of the electrolyte in CHF_2CF_3, the phase-transition pressure at 393.15 K is 6.0 MPa and 6.9 MPa, respectively, for $[N(^nC_4H_9)_4][B\{(3,5\text{-}CF_3)_2C_6H_3\}_4]$ and $[N(^nC_4H_9)_4][BF_4]$.

3.2 Electrical Conductivity

3.2.1 Effects of pressure on the molar conductivity of the CH_2F_2 systems. The electrical conductivity of the 8 salts (Table 1) were studied in CH_2F_2 at a fixed temperature of 363 K and in the pressure range between 9 MPa and 24 MPa. The first series of tests have been carried out for the mixtures with the same concentration of ~10 mmol dm^{-3}, see Figure 7. It can be seen that the molar conductivity of all electrolytes increases with pressure in the range of 9-24 MPa. This overall trend as a function of pressure results from the following two factors. Firstly, the dielectric constant of CH_2F_2 increases from 6.71 at 8.1 MPa to 9.59 at 26.1 MPa at 363 K,[11] which will affect the association/dissociation of the electrolytes, and hence the molar conductivity of the solution. Because the increase of dielectric constant is not linear with the pressure (faster below 12 MPa and slower above 12 MPa at 363 K), the increase of molar conductivity is also more significant at the low pressure range. Secondly, the viscosity of the fluid mixture increases with pressure, which tends to decrease the molar conductivity of the system.[30-32] This reverse effect may cancel out the dielectric constant effect to the molar conductivity at higher pressure, which is also a possible reason for the line to level out for $[N(^nC_4H_9)_4][Al(OC(CF_3)_3)_4]$ with c = 9.0 mmol dm^{-3} when the pressure is above 14 MPa.

The pressure effect on the molar conductivity also depends on the size of the anion in the electrolyte. As observed in our previous studies of the tetrafluoroborate and fluorinated tetraphenylborate compounds, the molar conductivity shows less pressure dependence with larger anions.[20] This conclusion also applies to all 8 electrolytes in the current study. It can be seen that for the electrolyte with the largest anion, $[N(^nC_4H_9)_4][Al(OC(CF_3)_3)_4]$, the molar conductivity almost remains the same when the system pressure increases from 14 to 24 MPa. The pressure effects becomes more pronounced for the two compounds with $[FAP]^-$ ($[N(^nC_4H_9)_4][FAP]$ and $[N(CH_3)_4][FAP]$) and for the three electrolytes with $[NTf_2]^-$ ($[N(^nC_4H_9)_4][NTf_2]$, [BMIM][NTf_2], and [EMIM][NTf_2]). When it comes to the two chlorides, [EMIM]Cl and $[N(^nC_4H_9)_4]Cl$, the molar conductivity of the systems almost increases linearly with pressure. The pressure dependence of the molar conductivity shown here provides useful information for choosing the operating pressure for carrying out electrodeposition.

3.2.2 Effects of different cations and anions on the molar conductivity of the CH_2F_2 systems. The 8 electrolytes have been directly compared and evaluated by using the molar conductivity at the same temperature, pressure and concentration. Table 2 lists the molar conductivity

of the electrolytes in CH_2F_2 at 363 K and 20 MPa, interpolated from the data shown in Figure 7. The following overall trend can be observed for the molar conductivity.

$[N(^nC_4H_9)_4][Al(OC(CF_3)_3)_4]$ > $[N(^nC_4H_9)_4][FAP]$ > $[N(CH_3)_4][FAP]$ > $[N(^nC_4H_9)_4][NTf_2]$ > $[BMIM][NTf_2]$ ≈ $[EMIM][NTf_2]$ > $[N(^nC_4H_9)_4]Cl$ > [EMIM]Cl

Furthermore, Figure 8 illustrates how the choice of the cations/anion affects the molar conductivity using 363 K and 20 MPa as the benchmark condition. For the four electrolytes with $[N(^nC_4H_9)_4]^+$, the molar conductivity increases with the radius of the anion, i.e. $[N(^nC_4H_9)_4]Cl$ < $[N(^nC_4H_9)_4][NTf_2]$ < $[N(^nC_4H_9)_4][FAP]$ < $[N(^nC_4H_9)_4][Al(OC(CF_3)_3)_4]$ (see Figure 8a). $[N(^nC_4H_9)_4][Al(OC(CF_3)_3)_4]$ has the highest molar conductivity (2.22×10^{-2} S m^2 mol^{-1}), higher than that of the two $[BAr^F]^-$ electrolytes we reported previously (i.e. 1.70×10^{-2} S m^2 mol^{-1} for $[N(^nC_4H_9)_4][B(C_6F_5)_4]$ and 1.97×10^{-2} S m^2 mol^{-1} for $[N(^nC_4H_9)_4][B\{3,5\text{-}C_6H_3(CF_3)_2\}_4]$[20]). The molar conductivity of the fluorinated aluminate is also nearly double that of the widely used commercial electrolyte $[N(^nC_4H_9)_4][BF_4]$ (1.24×10^{-2} S m^2 mol^{-1} at 20 MPa) in $scCH_2F_2$ under similar conditions.[17]

When using $[EMIM]^+$ as the cation, the molar conductivity of $[EMIM][NTf_2]$ is 5 times of that of the chloride (see Table 2 and Figure 8b). Similar to the solubility of the two $[EMIM]^+$ electrolytes, the highly fluorinated anion can significantly increase the molar conductivity of the $[EMIM]^+$ electrolyte in $scCH_2F_2$.

The two compounds with $[FAP]^-$, i.e. $[N(^nC_4H_9)_4][FAP]$ (1.64×10^{-2} S m^2 mol^{-1}) and $[N(CH_3)_4][FAP]$ (1.49×10^{-2} S m^2 mol^{-1}) show comparable molar conductivity to the $[BAr^F]^-$ electrolytes. It can also be seen from Figure 8d that with the same $[FAP]^-$ anion, the one with larger cation, $[N(^nC_4H_9)_4][FAP]$, has higher molar conductivity than that of $[N(CH_3)_4][FAP]$, suggesting that there are more dissociated ions/triple ions in the $[N(^nC_4H_9)_4][FAP]$ solution than in the $[N(CH_3)_4][FAP]$ solution under these conditions. However, this is not the case with the two $[NTf_2]^-$ electrolytes ($[BMIM][NTf_2]$ and $[EMIM][NTf_2]$), which have almost the same molar conductivity (Figure 8c) when one of the side alkyl chain of the imidazole ring changes from C_2H_5 to $^nC_4H_9$. We can also see from Figure 8c that the symmetrical ammonium cation ($[N(^nC_4H_9)_4]^+$) is better than the two imidazolium cations in terms of having the high conductivity for the $[NTf_2]^-$ electrolytes in $scCH_2F_2$.

Compared with the electrolytes with $[FAP]^-$ and $[NTf_2]^-$, the two chloride salts ($[N(^nC_4H_9)_4]Cl$ and [EMIM]Cl) show much lower molar conductivity under our experimental conditions (Figure 8c-8e). Consequently, the choice of the cation becomes critical for the chloride salts. When replacing

$[EMIM]^+$ with $[N(^nC_4H_9)_4]^+$, the enhancement in molar conductivity is $\Lambda_{[N(C_4H_9)_4]Cl}/\Lambda_{[EMIM][Cl]} = 4.1$ for the chlorides, whereas the enhancement factor (i.e. $\Lambda_{[N(C_4H_9)_4][NTf_2]}/\Lambda_{[EMIM][NTf_2]}$) is only 1.4 for the two $[NTf_2]^-$ electrolytes).

3.2.3 Effects of the concentration of supporting electrolytes on the molar conductivity of the CH_2F_2 systems. Since both $[N(^nC_4H_9)_4][Al(OC(CF_3)_3)_4]$ and $[N(^nC_4H_9)_4][FAP]$ have the highest molar conductivities in CH_2F_2 among the 8 electrolytes, detailed conductivity studies at various concentrations were carried out with these two compounds. It can be clearly seen from Figures 9 and 10 that for both electrolytes, the conductivity of the solutions increases with the concentration of the electrolytes (1-80 mmol dm^{-3}) over the entire pressure range from 9 to 24 MPa. The pressure effect on the conductivity is more pronounced with the $[N(^nC_4H_9)_4][FAP]$ + CH_2F_2 system, which shows continuous increases of the conductivity with pressure over the entire pressure range. The conductivity of the $[N(^nC_4H_9)_4][Al(OC(CF_3)_3)_4]$ + CH_2F_2 system however, only shows moderate pressure effects at low pressure region (9-13 MPa). The conductivity almost remains constant when the system pressure increase from 13 to 24 MPa. Comparing $[N(^nC_4H_9)_4][Al(OC(CF_3)_3)_4]$ and $[N(^nC_4H_9)_4][FAP]$, the stronger pressure effect with $[N(^nC_4H_9)_4][FAP]$ implies that its association /dissociation is more affected by the solvation shell than in $[N(^nC_4H_9)_4][Al(OC(CF_3)_3)_4]$.

To compare the conductivity behaviour of the four tetrabutylammonium electrolytes in CH_2F_2 over the concentration range used for the SCFED processes, the molar conductivity at 20 MPa is plotted against the square root of concentration, as shown in Figure 11. It can be seen that for $[N(^nC_4H_9)_4][Al(OC(CF_3)_3)_4]$ and $[N(^nC_4H_9)_4][FAP]$, the molar conductivity of the solutions decreases with increasing $\sqrt{c}$ and no minimum is observed in the concentration range studied. This behaviour is similar to that of the $[N(^nC_4H_9)_4][B\{3,5\text{-}C_6H_3(CF_3)_2\}_4]$ + CH_2F_2 system.[20] However, the Λ–$\sqrt{c}$ curves start to level out at high concentrations for the other two electrolytes when c > 20 mmol dm^{-3} for $[N(^nC_4H_9)_4][BF_4]$[17] or when c > 50 mmol dm^{-3} for $[N(^nC_4H_9)_4]Cl$. It was reported by Abbott et al.[17] that triple ions have a considerable contribution to the conductivity of $[N(^nC_4H_9)_4][BF_4]$ in CH_2F_2 at 363 K and 20 MPa (triple ion dissociation constant, K_T = ~60 mmol dm^{-3}). The molar conductivity data for $[N(^nC_4H_9)_4]Cl$ reported here may also suggest that the contribution from triple ions plays a part in its conductivity in CH_2F_2 at high concentrations. However, further work would be need to fully elucidate this. The molar conductivity data at low concentrations (<1 mmol dm^{-3}) are not available due to the difficulties in preparing very dilute mixtures with accurate concentration, hence the limiting molar conductivity of these compounds cannot be calculated reliably from the Λ–$\sqrt{c}$ curves.

The molar conductivity of $[N(^nC_4H_9)_4][Al(OC(CF_3)_3)_4]$ in CH_2F_2 is comparable to that of the previously studied $[N(^nC_4H_9)_4][B\{3,5\text{-}C_6H_3(CF_3)_2\}_4]$ + CH_2F_2 at all concentrations, making it an

excellent candidate for use in CH_2F_2 for electrodepositions. For $[N(^nC_4H_9)_4][FAP]$, although slightly lower than $[N(^nC_4H_9)_4][Al(OC(CF_3)_3)_4]$, its molar conductivity is still much higher than that of the routinely used $[N(^nC_4H_9)_4][BF_4]$, especially at high concentrations (e.g. at 20 mmol dm^{-3}, the molar conductivity of $[N(^nC_4H_9)_4][FAP]$ is 1.43×10^{-2} S m^2 mol^{-1} at 20 MPa and 363K, thus more than double the molar conductivity of $[N(^nC_4H_9)_4][BF_4]$, which is only 6.6×10^{-3} S m^2 mol^{-1} under similar conditions). This also makes $[N(^nC_4H_9)_4][FAP]$ a good electrolyte for SCFED.

Although $[N(^nC_4H_9)_4]Cl$ has the lowest molar conductivity over the concentration range between 1 and 80 mmol dm^{-3} among the 4 electrolytes depicted in Figure 11, our results indicate that $[N(^nC_4H_9)_4]Cl$ can be used as the support electrolyte when its concentration is high in the electrodeposition bath because it is highly soluble in CH_2F_2 (see Figure 4a) and its molar conductivity does not decrease significantly when c > 50 mmol dm^{-3}. For example, $[N(^nC_4H_9)_4]Cl$ can achieve 0.24 S m^{-1} for the conductivity from a solution of 60 mmol dm^{-3} at 363 K and 20 MPa, compared with the conductivity of 0.17 S m^{-1} obtained from the mixture of $[N(^nC_4H_9)_4][BF_4]$ + CH_2F_2 with the concentration of 25 mmol dm^{-3}, reported previously.[17]

3.2.4 Effects of a high critical temperature HFC (CHF_2CH_3) on the molar conductivity of $[N(^nC_4H_9)_4][BF_4]$ and $[N(^nC_4H_9)_4][B\{(3,5\text{-}CF_3)_2C_6H_3\}_4]$. Although the T_c of CHF_2CH_3 is 35 K higher than that of CH_2F_2, it is expected that both fluids will show similar behaviour in some of the thermodynamic properties (e.g. density) at the same reduced temperature ($T_r = T/T_c$). However, since the temperature has a dominant effect on the conductivity of the mixture with a given composition, we therefore chose a fixed temperature of 393.15 K to examine the difference between CHF_2CH_3 and CH_2F_2 on the molar conductivity of the supporting electrolytes. The results presented in this section reflect the combined effects of pressure/density and the chemical structures of the HFC on the molar conductivity.

The measurements of the molar conductivity were made for both $[N(^nC_4H_9)_4][BF_4]$ and $[N(^nC_4H_9)_4][B\{(3,5\text{-}CF_3)_2C_6H_3\}_4]$ in CHF_2CH_3 at 393.15 K (see Fig. 12a). The conductivity of $[N(^nC_4H_9)_4][BF_4]$ in CHF_2CH_3 increases monotonically as pressure increases in the tested pressure range between 8 and 24 MPa, whereas the Λ-p curve for the $[N(^nC_4H_9)_4][B\{(3,5\text{-}CF_3)_2C_6H_3\}_4]$ + CHF_2CH_3 mixture shows a small pressure effect on the conductivity over same pressure range. A shallow maximum in conductivity can be observed at ~15 MPa, resulting from the opposite effects on the conductivity induced by dielectric constant and viscosity with increasing the system pressure/density. For comparison with the conductivity in two HFCs at the same temperature, new conductivity measurements were also made at 393.15 K for the two electrolytes in CH_2F_2, see Fig. 12a. The molar conductivity increases with the increase of pressure for both $[N(^nC_4H_9)_4][BF_4]$ and $[N(^nC_4H_9)_4][B\{(3,5\text{-}CF_3)_2C_6H_3\}_4]$ over the entire measured pressure range in CH_2F_2. Based on the

phase diagrams show in Fig. 5a and in our previous work,[20] no conductivity data were collected below 14.5 MPa due to the possible phase separation at low pressures.

For experiments that used either $[N(^nC_4H_9)_4][BF_4]$ or $[N(^nC_4H_9)_4][B\{(3,5\text{-}CF_3)_2C_6H_3\}_4]$ as the supporting electrolyte, the two Λ-p curves obtained from CH_2F_2 and CHF_2CH_3, respectively, show a cross-over point. Below the pressure at the cross-over point, the conductivity in CHF_2CH_3 is higher than that in CH_2F_2, whereas the conductivity in CH_2F_2 is above that in CHF_2CH_3 when pressure is beyond the cross-over pressure. This behaviour is linked to the densities of the two HFCs in the supercritical region. Fig. 12b illustrates how the molar density of both CH_2F_2 and CHF_2CH_3 changes as a function of pressure at 393.15 K. The two isotherms intersect each other at 13.6 MPa. Below the cross-over pressure, the molar density of CHF_2CH_3 is higher than that of CH_2F_2, reflecting to the high conductivity of the two electrolytes in CHF_2CH_3 at low pressures. The cross-over pressures are 15.5 MPa and 17.8 MPa for the $[N(^nC_4H_9)_4][B\{(3,5\text{-}CF_3)_2C_6H_3\}_4]$ and $[N(^nC_4H_9)_4][BF_4]$ systems, respectively, both of which are higher than the cross-over pressure shown in the density isotherms. The shift of the cross-over pressure results from the changes in density, dielectric constant and viscosity when adding a small amount of electrolyte in the two HFCs. Although the test temperature of our conductivity measurements was limited to 393.15 K. Moreover, the conductivity of $[N(^nC_4H_9)_4][BF_4]$ is ~25% of that of $[N(^nC_4H_9)_4][B\{(3,5\text{-}CF_3)_2C_6H_3\}_4]$ in CHF_2CH_3 at 393.15 K and 20 MPa, suggesting that the $[N(^nC_4H_9)_4][B\{(3,5\text{-}CF_3)_2C_6H_3\}_4]$ salt is the preferred supporting electrolyte in scCHF_2CH_3, in terms of providing an electrodeposition bath with high conductivity.

4 Conclusions

Using low-polarity SCFs as a solvent for electrochemical processes, including electrodeposition in extreme nano-pores is a major challenge because of the low solubility and low conductivity of ionic compounds in such fluids. This work has progressed significantly from the stage of finding a usable supporting electrolyte/SCF, to that of using bulky substituents to achieve high conductivity for supporting large currents during the deposition process. In this study, we presented fundamental measurements of the phase behaviour and conductivities of a variety of the newly developed, task-specific electrolyte systems, which potentially broadens the materials that can be deposited from SCFs and are expected to improve the quality of the deposited materials. The need for task-specific electrolyte systems is illustrated by $[N(^nC_4H_9)_4][Al(OC(CF_3)_3)_4]$, and can potentially be used for high-temperature SCFED, while $[N(^nC_4H_9)_4]Cl$ is compatible with the halometallate salts used as the precursors for electrodeposition of a range of p-block elements, simplifying the solution speciation. By comparing the *p-T* phase boundaries between the one- to two- phase regions of the 8 binary systems in CH_2F_2, we have found that except for [EMIM]Cl + CH_2F_2, which requires notably higher

pressure to reach one phase condition at high temperature, the other seven compounds ($[N(^nC_4H_9)_4][Al(OC(CF_3)_3)_4]$, $[N(^nC_4H_9)_4][FAP]$, $[N(CH_3)_4][FAP]$, $[N(^nC_4H_9)_4][NTf_2]$, [BMIM][NTf_2], [EMIM][NTf_2] and $[N(^nC_4H_9)_4]Cl$) all exhibit moderate solubility in CH_2F_2. The comparison of the molar conductivity at ~10 mmol dm^{-3} shows that the $[N(^nC_4H_9)_4][Al(OC(CF_3)_3)_4]^+$ CH_2F_2 system exhibits the highest molar conductivity (2.22×10^{-2} S m^2 mol^{-1}) among the studied systems, including the previously reported ammonium fluorinated tetra-arylborate electrolytes. The two binary systems with the $[FAP]^-$ anions (i.e. $[N(^nC_4H_9)_4][FAP]$ + CH_2F_2 and $[N(CH_3)_4][FAP]$ + CH_2F_2) also show comparable molar conductivity to the previously used $[N(^nC_4H_9)_4][B\{(3,5\text{-}CF_3)_2C_6H_3\}_4]$ + CH_2F_2 at similar conditions. High concentrations of $[N(^nC_4H_9)_4]Cl$ ($c > 50$ mmol dm^{-3}) are recommended when using $[N(^nC_4H_9)_4]Cl$ as the supporting electrolyte in CH_2F_2 due to its relatively low molar conductivity (4.0×10^{-3} S m^2 mol^{-1} at 60 mmol dm^{-3}) and but high solubility in CH_2F_2.

CHF_2CH_3 provides an alternative to increasing the temperature of the electrodeposition bath without applying extreme high-pressure conditions, thus facilitating deposition at higher temperatures. $[N(^nC_4H_9)_4][BF_4]$ is much more soluble in CHF_2CH_3 than in CH_2F_2 at 393.15 K over a wide composition range. At a fixed temperature of 398.15 K, CHF_2CH_3 gives higher molar conductivity than CH_2F_2 at low pressure (below the cross-over pressure, see Figure 12). $[N(^nC_4H_9)_4][BF_4]$ has a much lower molar conductivity (~25%) than $[N(^nC_4H_9)_4][B\{(3,5\text{-}CF_3)_2C_6H_3\}_4]$ in CHF_2CH_3 at 393.15 K and 20 MPa, indicating that the $[N(^nC_4H_9)_4][B\{(3,5\text{-}CF_3)_2C_6H_3\}_4]$ salt is the preferential supporting electrolyte for the SCFED process using $scCHF_2CH_3$.

Acknowledgements

We thank EPSRC for financial support under a Programme Grant (EP/I033394/1). The SCFED Project (www.scfed.net) is a multidisciplinary collaboration of British universities investigating the fundamental and applied aspects of supercritical fluids. We are grateful to Messrs. M. Guyler, R. Wilson, P. Fields, D. Litchfield, and J. Warren for technical support. MWG acknowledges receipt of a Wolfson Research Merit Award. NS thanks Dr. D. S. Mitchell for helpful discussion and Ministry of Education of Malaysia for the studentship.

References

1 P. L. Dhepe, A. Fukuoka and M. Ichikawa, *Phys. Chem. Chem. Phys.*, 2003, **5**, 5565-5573.

2 N. Hasan and B. Farouk, *J. Supercrit. Fluids*, 2013, **80**, 60-70.

3 D. Cook, P. N. Bartlett, W. Zhang, W. Levason, G. Reid, J. Ke, W. Su, M. W. George, J. Wilson, D. Smith, K. Mallik, E. Barrett and P. Sazio, *Phys. Chem. Chem. Phys.*, 2010, **12**, 11744-11752.

4 J. Ke, P. N. Bartlett, D. Cook, T. L. Easun, M. W. George, W. Levason, G. Reid, D. Smith, W. Su and W. Zhang, *Phys. Chem. Chem. Phys.*, 2012, **14**, 1517-1528.

5 P. N. Bartlett, M. Perdjon-Abel, D. Cook, G. Reid, W. Levason, F. Cheng, W. Zhang, M. W. George, J. Ke, R. Beanland and J. Sloan, *ChemElectroChem*, 2014, **1**, 187-194.

6 C. Y. Cummings, P. N. Bartlett, D. Pugh, G. Reid, W. Levason, M. M. Hasan, A. L. Hector, J. Spencer and D. C. Smith, *J. Electrochem. Soc.*, 2015, **162**, D619-D624.

7 P. N. Bartlett, J. Burt, D. A. Cook, C. Y. Cummings, M. W. George, A. L. Hector, M. M. Hasan, J. Ke, W. Levason, D. Pugh, G. Reid, P. W. Richardson, D. C. Smith, J. Spencer, N. Suleiman and W. Zhang, *Chem. - Eur. J.*, 2016, **22**, 302-309.

8 J. Ke, W. Su, S. M. Howdle, M. W. George, D. Cook, M. Perdjon-Abel, P. N. Bartlett, W. Zhang, F. Cheng, W. Levason, G. Reid, J. Hyde, J. Wilson, D. C. Smith, K. Mallik and P. Sazio, *Proc. Natl. Acad. Sci. U. S. A.*, 2009, **106**, 14768-14772, S14768/14761-S14768/14765.

9 D. Niehaus, M. Philips, A. Michael and R. M. Wightman, *J. Phys. Chem.*, 1989, **93**, 6232-6236.

10 A. P. Abbott and J. C. Harper, *J. Chem. Soc., Faraday Trans.*, 1996, **92**, 3895-3898.

11 A. P. Abbott, C. A. Eardley and R. Tooth, *J. Chem. Eng. Data*, 1999, **44**, 112-115.

12 A. P. Abbott, C. A. Eardley, J. C. Harper and E. G. Hope, *J. Electroanal. Chem.*, 1998, **457**, 1-4.

13 C. W. Meyer and G. Morrison, *J. Phys. Chem.*, 1991, **95**, 3860-3866.

14 M. T. Barão, U. V. Mardolcar and C. A. Nieto de Castro, *Fluid Phase Equilib.*, 1998, **150–151**, 753-762.

15 S. A. Olsen and D. E. Tallman, *Anal. Chem*, 1994, **66**, 503-509.

16 S. A. Olsen and D. E. Tallman, *Anal. Chem.*, 1996, **68**, 2054-2061.

17 A. P. Abbott and C. A. Eardley, *J. Phys. Chem. B*, 2000, **104**, 9351-9355.

18 P. N. Bartlett, D. A. Cook, M. W. George, A. L. Hector, J. Ke, W. Levason, G. Reid, D. C. Smith and W. Zhang, *Phys. Chem. Chem. Phys.*, 2014, **16**, 9202-9219.

19 P. N. Bartlett, D. C. Cook, M. W. George, J. Ke, W. Levason, G. Reid, W. Su and W. Zhang, *Phys. Chem. Chem. Phys.*, 2010, **12**, 492-501.

20 P. N. Bartlett, D. C. Cook, M. W. George, J. Ke, W. Levason, G. Reid, W. Su and W. Zhang, *Phys. Chem. Chem. Phys.*, 2011, **13**, 190-198.

21 R. L. David, *CRC Handbook of Chemistry and Physics, 89th Edition*, CRC Press/Taylor and Francis, Boca Raton, FL., 2009.

22 E. W. Lemmon, M. L. Huber and M. O. McLinden, *NIST Standard Reference Data 23 REFPROP Ver. 8.0*, 2007.

23 P. N. Bartlett, D. Cook, C. H. de Groot, A. L. Hector, R. Huang, A. Jolleys, G. P. Kissling, W. Levason, S. J. Pearce and G. Reid, *Rsc Advances*, 2013, **3**, 15645-15654.

24 A. P. Abbott and K. J. McKenzie, *Phys. Chem. Chem. Phys.*, 2006, **8**, 4265-4279.

25 S. Feja, *Int. J. Refrig.*, 2012, **35**, 1367-1371.

26 M. Atobe, S. Iizuka, R. Kobayakawa and T. Fuchigami, *J. Electrochem. Soc.*, 2010, **157**, E19-E23.

27 P. Licence, M. P. Dellar, R. G. M. Wilson, P. A. Fields, D. Litchfield, H. M. Woods, M. Poliakoff and S. M. Howdle, *Rev. of Sci. Instrum.*, 2004, **75**, 3233.

28 A. M. Feltham and M. Spiro, *Chem. Rev.*, 1971, **71**, 177-193.

29 R. Dohrn and G. Brunner, *Fluid Phase Equilib.*, 1995, **106**, 213-282.

30 A. P. Abbott, E. G. Hope and D. J. Palmer, *J. Phys. Chem. B*, 2007, **111**, 8114-8118.

31 A. P. Abbott, E. G. Hope and D. J. Palmer, *Anal. Chem.*, 2005, **77**, 6702-6708.

32 A. Laesecke and S. Bair, *Int. J. Thermophys.*, 2011, **32**, 925-941.

Table 1 Chemical structure of the ionic compounds

Abbreviation	Cation	Anion
[BMIM][NTf_2]	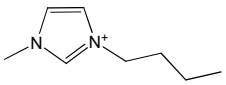	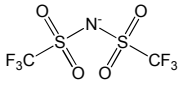
[EMIM][NTf_2]	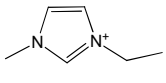	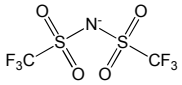
[EMIM][Cl]	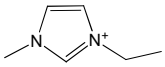	Cl-
[$N(^nC_4H_9)_4$][Cl]	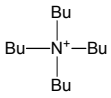	Cl-
[$N(^nC_4H_9)_4$][NTf_2]	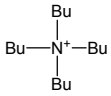	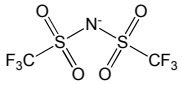
[$N(^nC_4H_9)_4$][FAP]	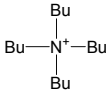	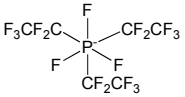
[$N(CH_3)_4$][FAP]	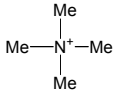	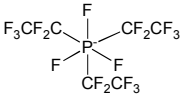
[$N(^nC_4H_9)_4$][$Al(OC(CF_3)_3)_4$]	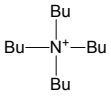	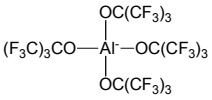
[$N(^nC_4H_9)_4$][BF_4]	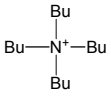	
[$N(^nC_4H_9)_4$][[B{(3,5-CF_3)$_2$$C_6H_3$}$_4$]	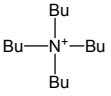	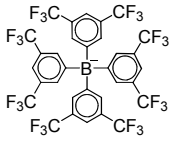

Table 2 Molar conductivity of the electrolytes in CH_2F_2 at 20 MPa and 363 K [a]

Electrolyte	$\Lambda \times 10^4/(S\ m^2\ mol^{-1})$
$[N(^nC_4H_9)_4][Al(OC(CF_3)_3)_4]$	222
$[N(^nC_4H_9)_4][FAP]$	164
$[N(CH_3)_4][FAP]$	149
$[N(^nC_4H_9)_4][NTf_2]$	99
$[BMIM][NTf_2]$	75
$[EMIM][NTf_2]$	73
$[N(^nC_4H_9)_4]Cl$	61
[EMIM]Cl	15

[a] The concentration of all of the electrolytes is ~10 mmol dm^{-3}. Polynomial regressions were used to interpolate the data shown in Figure 7 to the fixed pressure (20 MPa).

Figure Captions

Fig. 1 Schematic diagram of the experimental set-up for measuring conductivity of binary mixtures: CM, conductivity meter; E, platinum electrodes; EH, electrode holder; G, glass tube; HS, hollow screw; M, motor for driving the stirrer; MB, main body of the conductivity vessel; O, oil bath; P, pressure transducer; PH, pre-heater; S, stirrer; SE, PTFE seal; T, Pt 100 temperature sensor; V1, V2, valves. The thick dotted box represents the oil bath. The thin dotted lines indicate the devices which are connected to the computer for remote control and data recording.

Fig. 2 *p-T* phase diagram of the binary system of [EMIM][NTf_2] (1) + CH_2F_2 (2). ■, x_1= 0.19 × 10^{-3}; ●, x_1= 0.64 × 10^{-3}; ▲, x_1= 1.72 × 10^{-3}; ▼, x_1= 2.81 × 10^{-3}; ◆, x_1= 4.25 × 10^{-3}.

Fig. 3 The p-T phase diagram of the binary mixture of supporting electrolyte(1) + CH_2F_2(2). ▽, $[N(^nC_4H_9)_4][Al(OC(CF_3)_3)_4]$, x_1 = 4.3×10^{-4}; △, $[N(^nC_4H_9)_4][FAP]$, x_1 = 4.8×10^{-4}; ○, $[N(^nC_4H_9)_4][NTf_2]$, x_1 = 5.2 × 10^{-4}; □, $[N(^nC_4H_9)_4]Cl$, x_1 = 4.9×10^{-4}; +, [EMIM]Cl, x_1 = 4.7×10^{-4}; ×, [EMIM][NTf_2], x_1 = 6.4 × 10^{-4}; ●, [BMIM][NTf_2], x_1 = 3.9 × 10^{-4}; ✱, $[N(CH_3)_4][FAP]$, x_1 = 5.1×10^{-4}.

Fig. 4 (a) p-*x* phase diagram of the mixture at 363 K: ●, [EMIM][NTf_2] (1) + CH_2F_2 (2); ■, $[N(^nC_4H_9)_4][Al(OC(CF_3)_3)_4]$ (1) + CH_2F_2 (2); and ▲, $[N(^nC_4H_9)_4][Cl]$ (1) + CH_2F_2 (2). (b) *p-T* phase diagram of the binary mixture of $[N(^nC_4H_9)_4][Al(OC(CF_3)_3)_4]$(1) + CH_2F_2 (2) with x_1= 4.3×10^{-4} (□), 1.29×10^{-3} (○), x_1= 2.54×10^{-3} (△), x_1= 3.77×10^{-3} (▽), x_1= 5.27×10^{-3} (◇).

Fig. 5 (a) p–T phase diagrams of the binary mixtures of $[N(^nC_4H_9)_4][BF_4]$ + CHF_2CH_3 and $[N(^nC_4H_9)_4][BF_4]$ + CH_2F_2. $[N(^nC_4H_9)_4][BF_4]$(1) + CHF_2CH_3(2): ◆, x_1 = 1.67×10^{-3}; ●, x_1 = 4.01×10^{-3}; ▲, x_1 = 8.12×10^{-3}; ▼, x_1 = 15.8×10^{-3}. $[N(^nC_4H_9)_4][BF_4]$(1) + CH_2F_2(2): ◇, x_1 = 4.17×10^{-3}. (b) p–*x* phase diagrams of the binary mixtures at 393.15 K. ✚, $[N(^nC_4H_9)_4][BF_4]$ + CHF_2CH_3; ■, $[N(^nC_4H_9)_4][BF_4]$ + CH_2F_2, experimental phase transition pressure measured in this study; □, $[N(^nC_4H_9)_4][BF_4]$ + CH_2F_2, extrapolated phase transition pressures obtained from the previously reported data, the error bars represent the confidence interval of 95% for the extrapolated data.

Fig. 6 Comparison of the p–T phase diagram of the two binary mixtures. ■, $[N(^nC_4H_9)_4][BF_4]$(1) + CHF_2CH_3(2), x_1 = 1.67×10^{-3}; and ●, $[N(^nC_4H_9)_4][B\{(3,5\text{-}CF_3)_2C_6H_3\}_4]$(1) + CHF_2CH_3(2), x_1 = 1.65×10^{-3}. The tabulated phase equilibrium data shown in the figure can be found from Tables S4 and S5 in the supplementary information.

Fig. 7 Molar conductivity (Λ) of the electrolytes in CH_2F_2 at 363 K, the molar concentration of the electrolytes is ~10 mmol dm^{-3}. ■, $[N(^nC_4H_9)_4][Al(OC(CF_3)_3)_4]$, 9.0 mmol dm^{-3}; ●, $[N(^nC_4H_9)_4][FAP]$, 10.1 mmol dm^{-3}; ▲, $[N(CH_3)_4][FAP]$, 10.3 mmol dm^{-3}; ▼, $[N(^nC_4H_9)_4][NTf_2]$, 10.8 mmol dm^{-3}; ▶, [BMIM][NTf_2], 10.1 mmol dm^{-3}; ◀, [EMIM][NTf_2], 11.6 mmol dm^{-3}; ◆, $[N(^nC_4H_9)_4]$Cl, 8.4 mmol dm^{-3}; ★, [EMIM]Cl, 11.3 mmol dm^{-3}.

Fig. 8 Molar conductivity (Λ) of the electrolytes in CH_2F_2 at 363 K and 20 MPa. The molar conductivity data were interpolated from the corresponding Λ-p isotherm shown in Figure 5. (a) $[N(^nC_4H_9)_4]^+$ with four different anions, [Y] = Cl^-, $[NTf_2]^-$, $[FAP]^-$ and $[Al(OC(CF_3)_3)_4]^-$; (b) $[EMIM]^+$ with two different anions, [Y] = Cl^- and $[NTf_2]^-$; (c) $[NTf_2]^-$ with three different cations, [X] = $[N(^nC_4H_9)_4]^+$, $[BMIM]^+$ and $[EMIM]^+$; (d) $[FAP]^-$ with two different cations, [X] = $[N(^nC_4H_9)_4]^+$ and $[N(^nCH_3)_4]^+$; (e) Cl^- with two different cations, [X] = $[N(^nC_4H_9)_4]^+$ and $[EMIM]^+$. The y-axis in all of the 5 sub-panels have the same scale.

Fig. 9 Conductivity (κ) of $[N(^nC_4H_9)_4][Al(OC(CF_3)_3)_4]$ in CH_2F_2 at 363K. The molar concentrations of $[N(^nC_4H_9)_4][Al(OC(CF_3)_3)_4]$ are: ◭, 1.04 mmol dm^{-3}; ▷, 1.98 mmol dm^{-3}; ◁, 2.93 mmol dm^{-3}; ◇, 5.32 mmol dm^{-3}; ▽, 8.98 mmol dm^{-3}; △, 20.0 mmol dm^{-3}; ○, 38.8 mmol dm^{-3}; □, 59.8 mmol dm^{-3}.

Fig. 10 Conductivity (κ) of $[N(^nC_4H_9)_4][FAP]$ in CH_2F_2 at 363 K. The molar concentrations of $[N(^nC_4H_9)_4][FAP]$ are: ◭, 0.98 mmol dm^{-3}; ◭, 2.09 mmol dm^{-3}; ▷, 5.06 mmol dm^{-3}; ◁, 8.01 mmol dm^{-3}; ◇, 10.1 mmol dm^{-3}; ▽, 20.1 mmol dm^{-3}; △, 29.5 mmol dm^{-3}; ○, 49.7 mmol dm^{-3}; □, 80.7 mmol dm^{-3}.

Fig. 11 Molar conductivity (Λ) of $[N(^nC_4H_9)_4][Al(OC(CF_3)_3)_4]$ (■), $[N(^nC_4H_9)_4][FAP]$ (◆), $[N(^nC_4H_9)_4][BF_4]$ (▲)[17],and $[N(^nC_4H_9)_4]Cl$ (●) in CH_2F_2 at 20 MPa and 363K. The molar conductivities were obtained by interpolating the data shown in Figures 9 and 10 to the fixed pressure (20 MPa) using polynomial regressions. The lines are merely to guide the eye. The error bars represent the standard uncertainties for Λ, estimated from the experimental uncertainties of the conductivity measurements and the sample concentrations.

Fig. 12 (a) Molar conductivity (Λ) of $[N(^nC_4H_9)_4][BF_4]$ and $[N(^nC_4H_9)_4]$ $[B\{(3,5\text{-}CF_3)_2C_6H_3\}_4]$ in CHF_2CH_3 and CH_2F_2 at 393.15 K. □, $[N(^nC_4H_9)_4][BF_4]$ in CH_2F_2; ■, $[N(^nC_4H_9)_4][BF_4]$ in CHF_2CH_3; ○, $[N(^nC_4H_9)_4]$ $[B\{(3,5\text{-}CF_3)_2C_6H_3\}_4]$ in CH_2F_2; and ●, $[N(^nC_4H_9)_4]$ $[B\{(3,5\text{-}CF_3)_2C_6H_3\}_4]$ in CHF_2CH_3. The concentration of the electrolyte is ~9 mmol dm^{-3}. (b) The molar density (ρ) plotted as a function of pressure at 393.15 K. The solid and dashed lines represent the isotherms for CHF_2CH_3 and CH_2F_2, respectively.

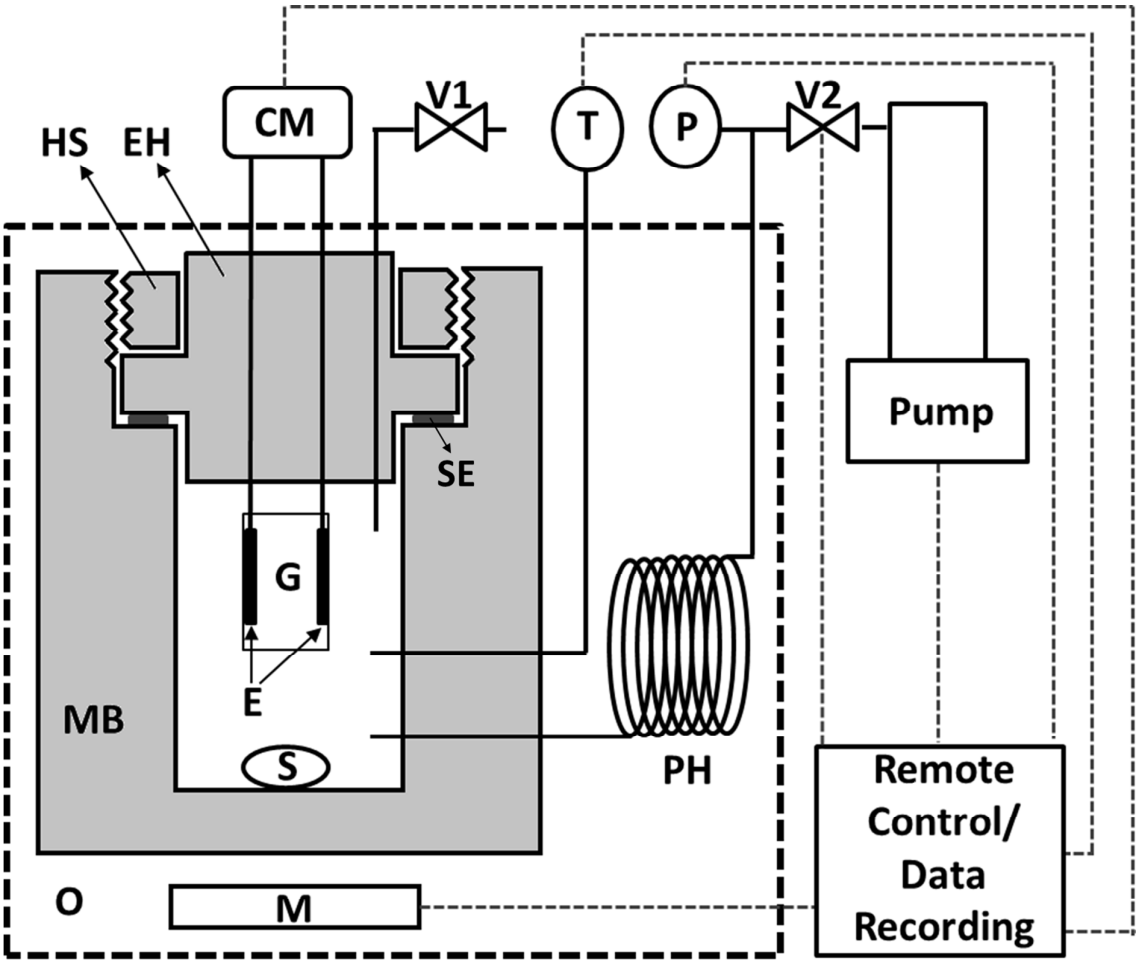

Fig. 1 Schematic diagram of the experimental set-up for measuring conductivity of binary mixtures: CM, conductivity meter; E, platinum electrodes; EH, electrode holder; G, glass tube; HS, hollow screw; M, motor for driving the stirrer; MB, main body of the conductivity vessel; O, oil bath; P, pressure transducer; PH, pre-heater; S, stirrer; SE, PTFE seal; T, Pt 100 temperature sensor; V1, V2, valves. The thick dotted box represents the oil bath. The thin dotted lines indicate the devices which are connected to the computer for remote control and data recording.

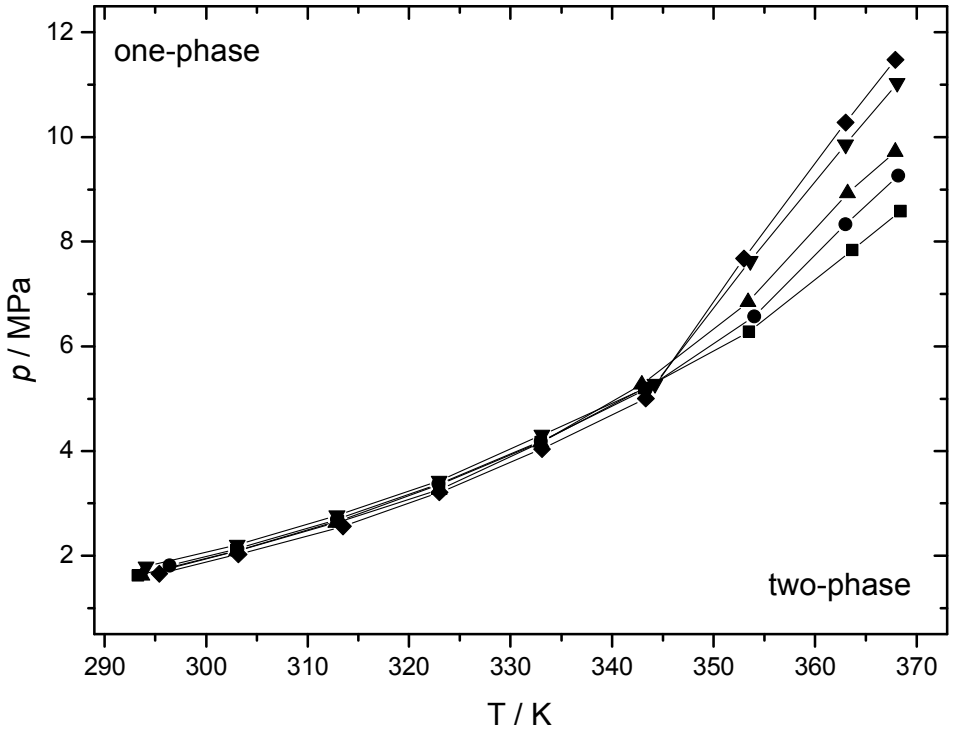

Fig. 2 *p*-*T* phase diagram of the binary system of [EMIM][NTf_2] (1) + CH_2F_2 (2). ■, x_1= 0.19 × 10^{-3}; ●, x_1= 0.64 × 10^{-3}; ▲, x_1= 1.72 × 10^{-3}; ▼ , x_1= 2.81 × 10^{-3}; ◆ , x_1= 4.25 × 10^{-3}.

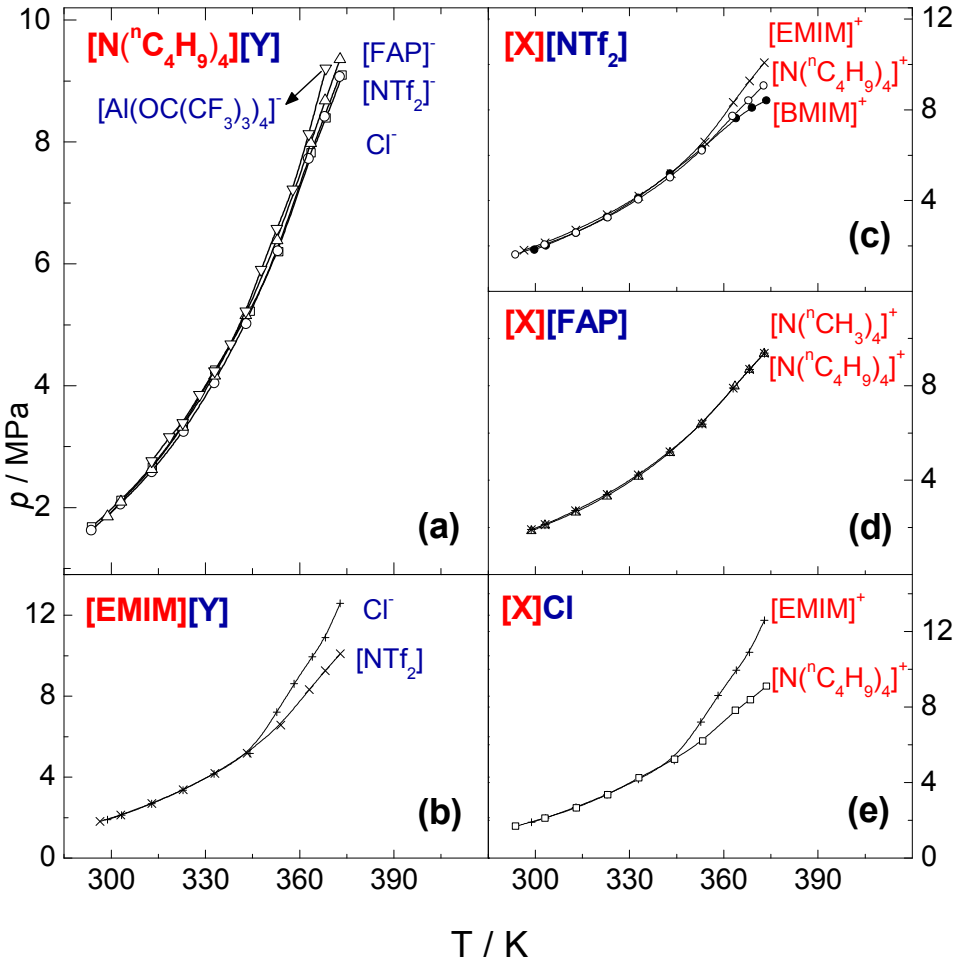

Fig. 3 The p-T phase diagram of the binary mixture of supporting electrolyte(1) + CH_2F_2(2). ▽, $[N(^nC_4H_9)_4][Al(OC(CF_3)_3)_4]$, x_1 = 4.3×10^{-4}; △, $[N(^nC_4H_9)_4][FAP]$, x_1 = 4.8×10^{-4}; ○, $[N(^nC_4H_9)_4][NTf_2]$, x_1 = 5.2 × 10^{-4}; □, $[N(^nC_4H_9)_4]Cl$, x_1 = 4.9×10^{-4}; +, [EMIM]Cl, x_1 = 4.7×10^{-4}; ×, $[EMIM][NTf_2]$, x_1 = 6.4 × 10^{-4}; ●, $[BMIM][NTf_2]$, x_1 = 3.9 × 10^{-4}; ✱, $[N(CH_3)_4][FAP]$, x_1 = 5.1×10^{-4}.

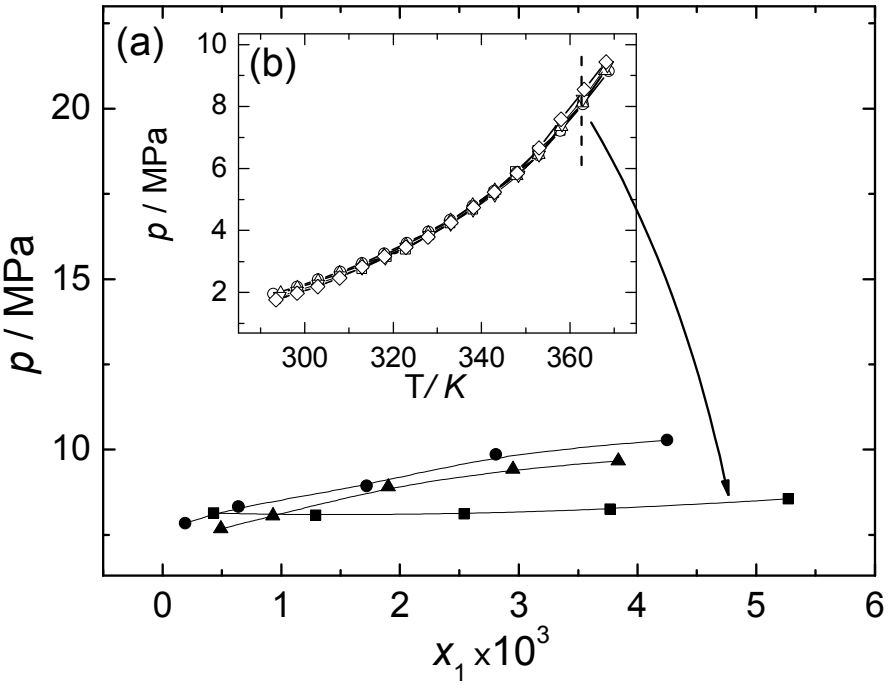

Fig. 4 (a) p-x phase diagram of the mixture at 363 K: ●, [EMIM][NTf_2] (1) + CH_2F_2 (2); ■, [$N(^nC_4H_9)_4$][$Al(OC(CF_3)_3)_4$] (1) + CH_2F_2 (2); and ▲, [$N(^nC_4H_9)_4$][Cl] (1) + CH_2F_2 (2). (b) p-T phase diagram of the binary mixture of [$N(^nC_4H_9)_4$][$Al(OC(CF_3)_3)_4$](1) + CH_2F_2 (2) with x_1= 4.3×10^{-4} (□), 1.29×10^{-3} (○), x_1= 2.54×10^{-3} (△), x_1= 3.77×10^{-3} (▽), x_1= 5.27×10^{-3} (◇).

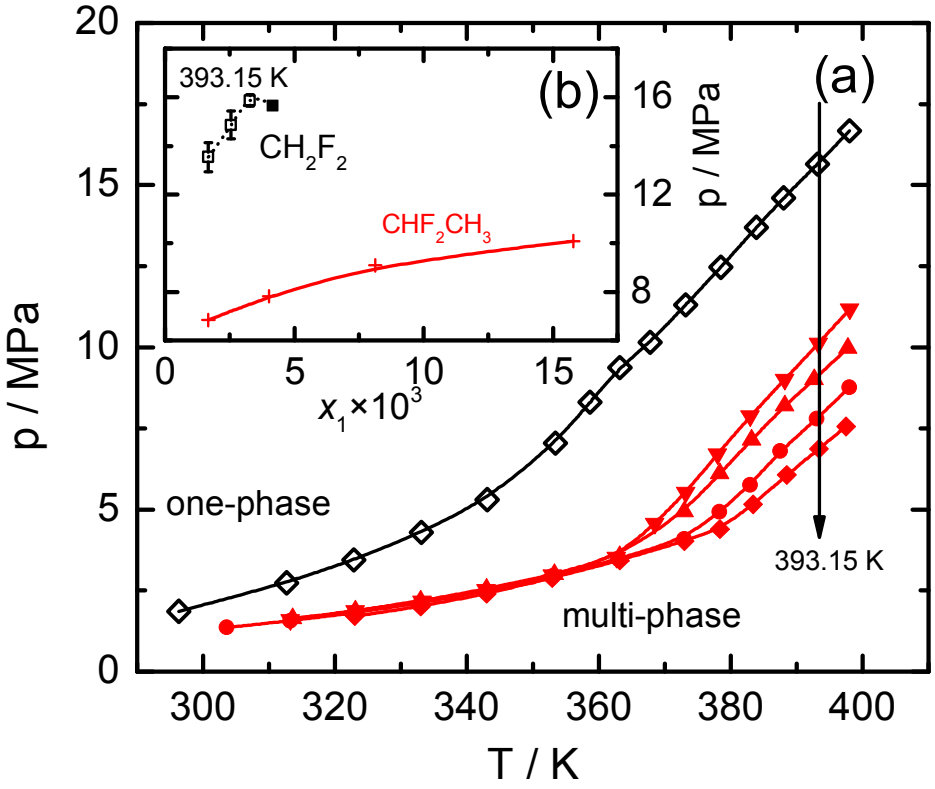

Fig. 5 (a) p–T phase diagrams of the binary mixtures of $[N(^nC_4H_9)_4][BF_4]$ + CHF_2CH_3 and $[N(^nC_4H_9)_4][BF_4]$ + CH_2F_2. $[N(^nC_4H_9)_4][BF_4](1)$ + $CHF_2CH_3(2)$: ◆, $x_1 = 1.67\times10^{-3}$; ●, $x_1 = 4.01\times10^{-3}$; ▲, $x_1 = 8.12\times10^{-3}$; ▼, $x_1 = 15.8\times10^{-3}$. $[N(^nC_4H_9)_4][BF_4](1)$ + $CH_2F_2(2)$: ◇, $x_1 = 4.17\times10^{-3}$. (b) p–x phase diagrams of the binary mixtures at 393.15 K. +, $[N(^nC_4H_9)_4][BF_4]$ + CHF_2CH_3; ■, $[N(^nC_4H_9)_4][BF_4]$ + CH_2F_2, experimental phase transition pressure measured in this study; □, $[N(^nC_4H_9)_4][BF_4]$ + CH_2F_2, extrapolated phase transition pressures obtained from the previously reported data, the error bars represent the confidence interval of 95% for the extrapolated data.

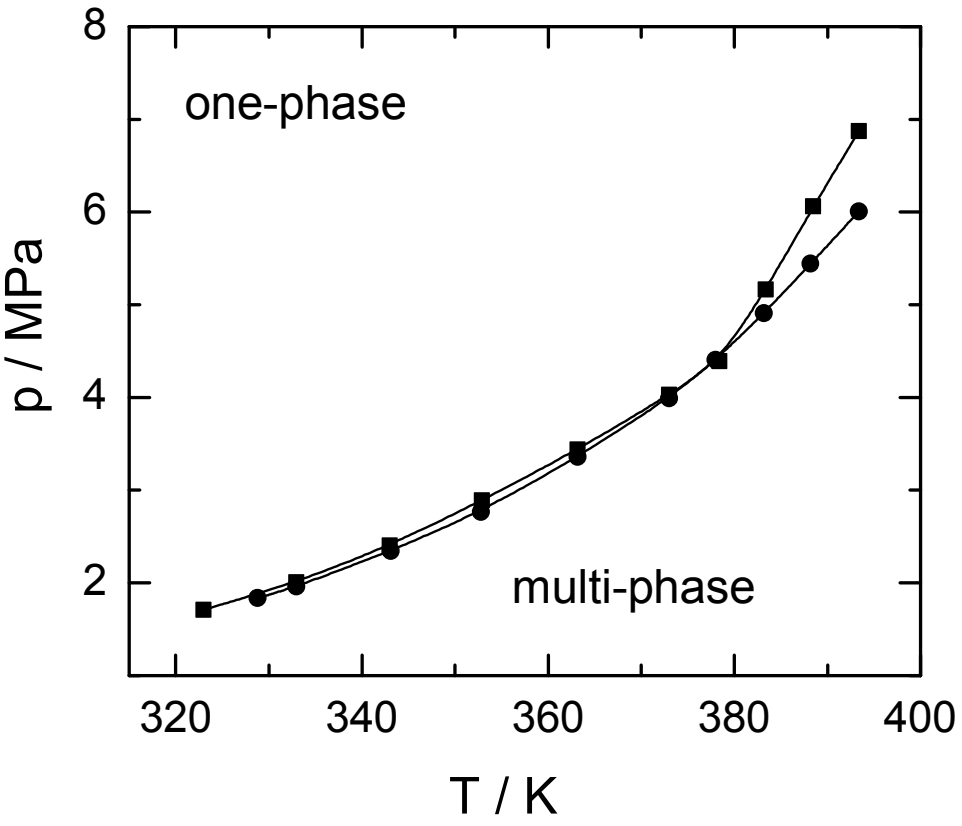

Fig. 6 Comparison of the p–T phase diagram of the two binary mixtures. ■, $[N(^nC_4H_9)_4][BF_4]$(1) + CHF_2CH_3(2), x_1 = 1.67×10^{-3}; and ●, $[N(^nC_4H_9)_4][B\{(3,5\text{-}CF_3)_2C_6H_3\}_4]$(1) + CHF_2CH_3(2), x_1 = 1.65×10^{-3}. The tabulated phase equilibrium data shown in the figure can be found from Tables S4 and S5 in the supplementary information.

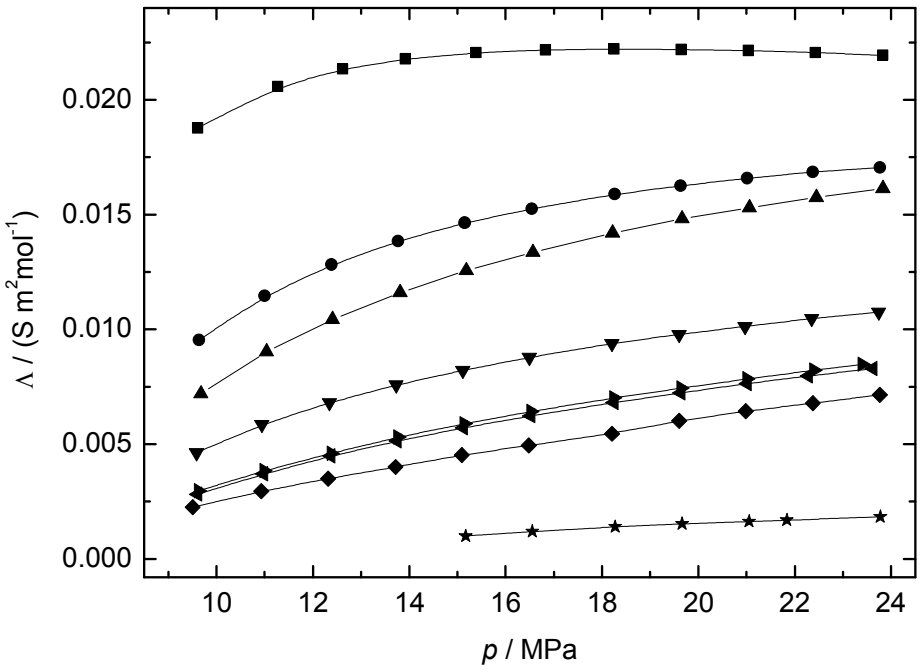

Fig. 7 Molar conductivity (Λ) of the electrolytes in CH_2F_2 at 363 K, the molar concentration of the electrolytes is ~10 mmol dm^{-3}. ■, $[N(^nC_4H_9)_4][Al(OC(CF_3)_3)_4]$, 9.0 mmol dm^{-3}; ●, $[N(^nC_4H_9)_4][FAP]$, 10.1 mmol dm^{-3}; ▲, $[N(CH_3)_4][FAP]$, 10.3 mmol dm^{-3}; ▼, $[N(^nC_4H_9)_4][NTf_2]$, 10.8 mmol dm^{-3}; ►, [BMIM][NTf_2], 10.1 mmol dm^{-3}; ◄, [EMIM][NTf_2], 11.6 mmol dm^{-3}; ◆, $[N(^nC_4H_9)_4]Cl$, 8.4 mmol dm^{-3}; ★, [EMIM]Cl, 11.3 mmol dm^{-3}.

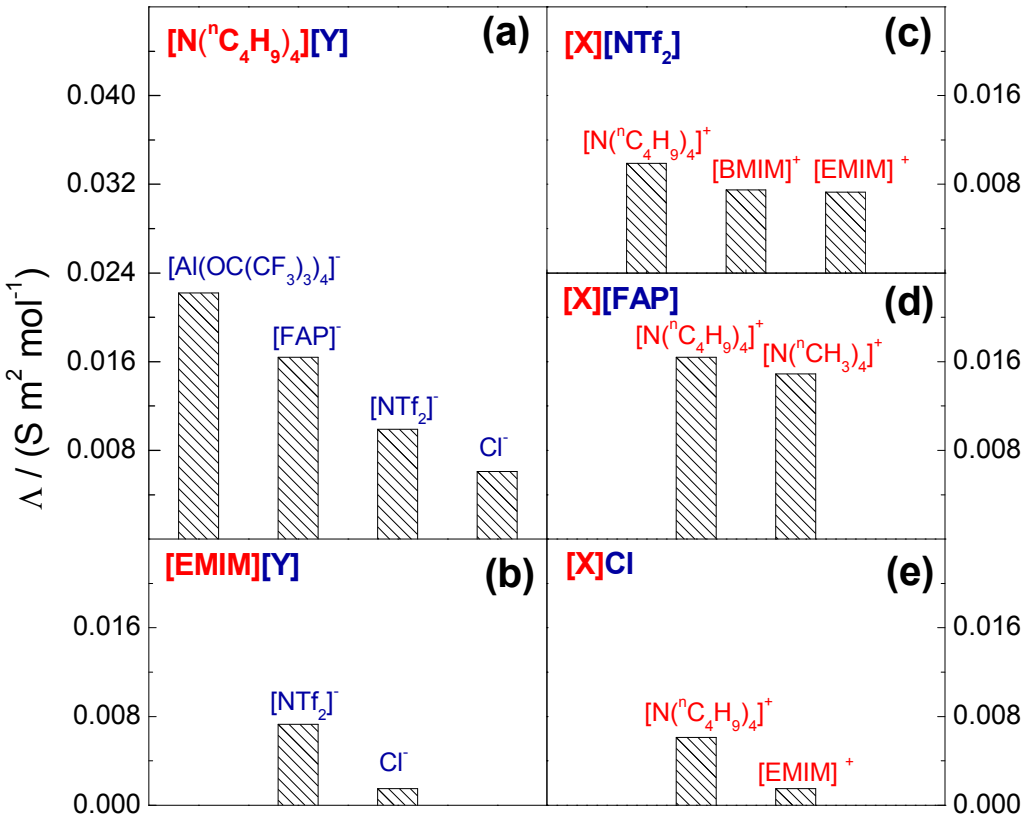

Fig. 8 Molar conductivity (Λ) of the electrolytes in CH_2F_2 at 363 K and 20 MPa. The molar conductivity data were interpolated from the corresponding Λ-p isotherm shown in Figure 5. (a) $[N(^nC_4H_9)_4]^+$ with four different anions, [Y] = Cl^-, $[NTf_2]^-$, $[FAP]^-$ and $[Al(OC(CF_3)_3)_4]^-$; (b) $[EMIM]^+$ with two different anions, [Y] = Cl^- and $[NTf_2]^-$; (c) $[NTf_2]^-$ with three different cations, [X] = $[N(^nC_4H_9)_4]^+$, $[BMIM]^+$ and $[EMIM]^+$; (d) $[FAP]^-$ with two different cations, [X] = $[N(^nC_4H_9)_4]^+$ and $[N(^nCH_3)_4]^+$; (e) Cl^- with two different cations, [X] = $[N(^nC_4H_9)_4]^+$ and $[EMIM]^+$. The y-axis in all of the 5 sub-panels have the same scale.

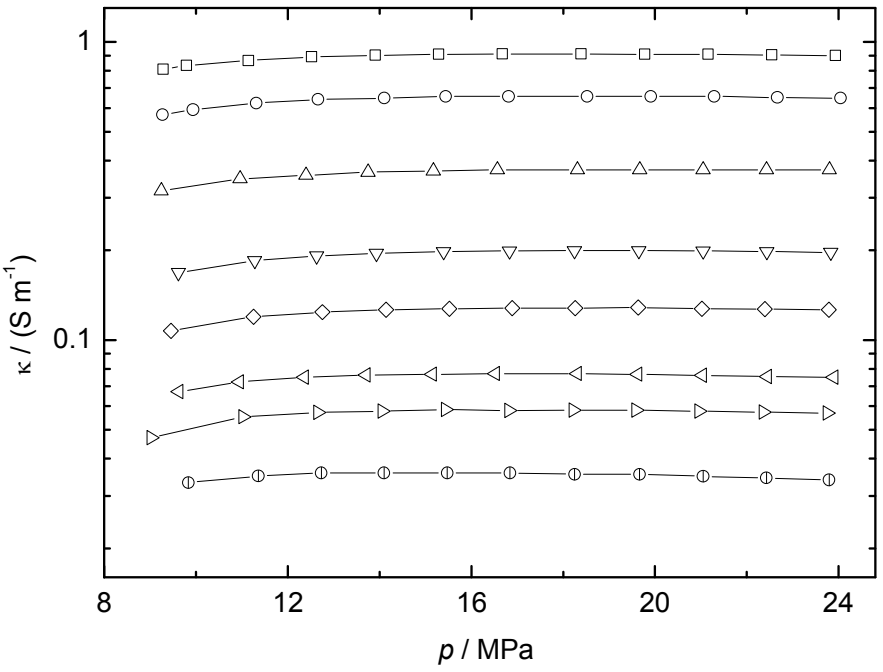

Fig. 9 Conductivity (κ) of $[N(^nC_4H_9)_4][Al(OC(CF_3)_3)_4]$ in CH_2F_2 at 363K. The molar concentrations of $[N(^nC_4H_9)_4][Al(OC(CF_3)_3)_4]$ are: ⦶, 1.04 mmol dm^{-3}; ▷, 1.98 mmol dm^{-3}; ◁, 2.93 mmol dm^{-3}; ◇, 5.32 mmol dm^{-3}; ▽, 8.98 mmol dm^{-3}; △, 20.0 mmol dm^{-3}; ○, 38.8 mmol dm^{-3}; □, 59.8 mmol dm^{-3}.

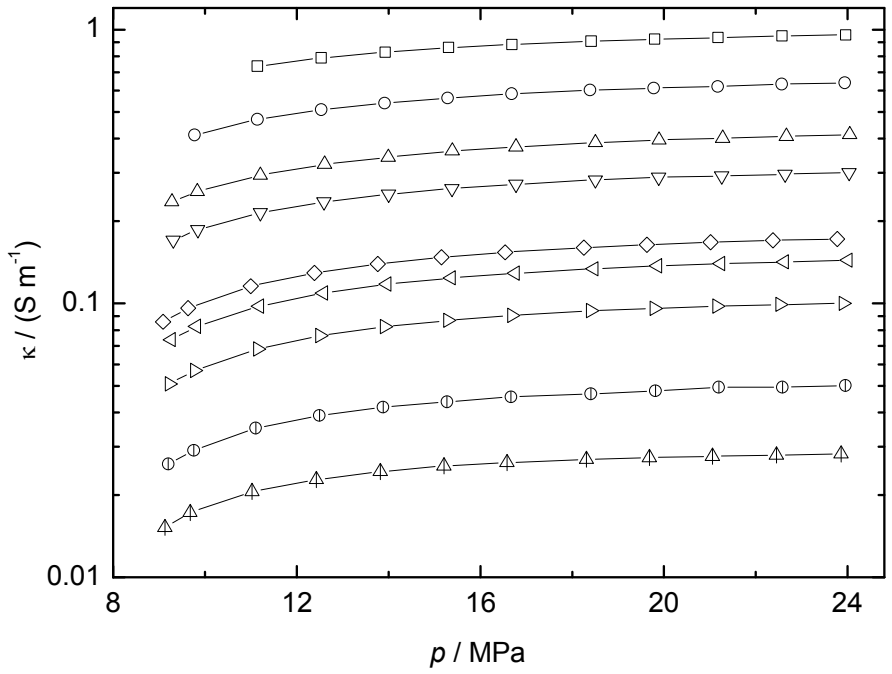

Fig. 10 Conductivity (κ) of $[N(^nC_4H_9)_4][FAP]$ in CH_2F_2 at 363 K. The molar concentrations of $[N(^nC_4H_9)_4][FAP]$ are: ◭, 0.98 mmol dm^{-3}; ◮, 2.09 mmol dm^{-3}; ▷, 5.06 mmol dm^{-3}; ◁, 8.01 mmol dm^{-3}; ◇, 10.1 mmol dm^{-3}; ▽, 20.1 mmol dm^{-3}; △, 29.5 mmol dm^{-3}; ○, 49.7 mmol dm^{-3}; ❑, 80.7 mmol dm^{-3}.

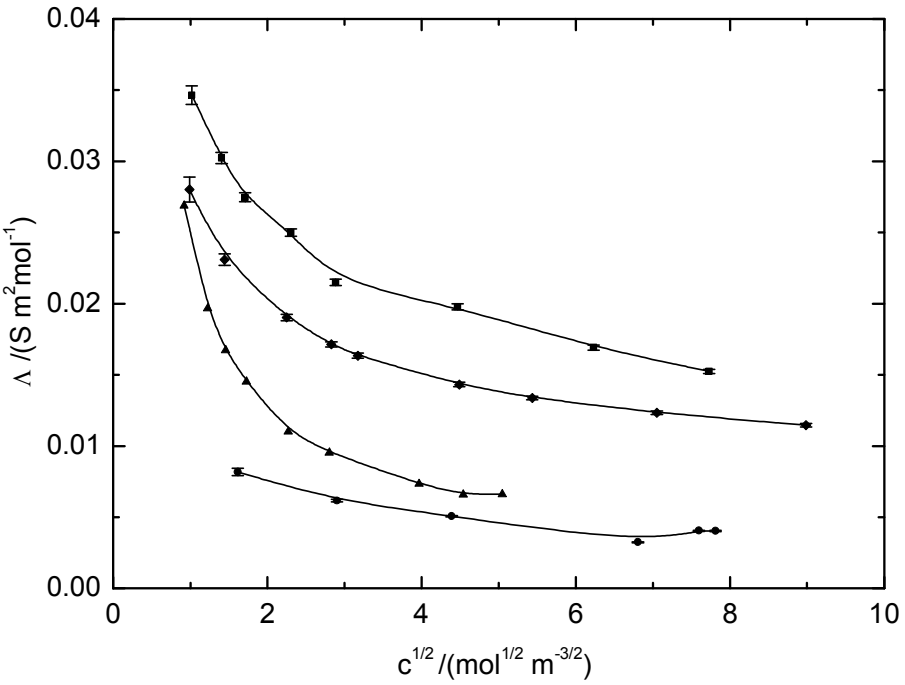

Fig. 11 Molar conductivity (Λ) of $[N(^nC_4H_9)_4][Al(OC(CF_3)_3)_4]$ (■), $[N(^nC_4H_9)_4][FAP]$ (◆), $[N(^nC_4H_9)_4][BF_4]$ (▲)[17],and $[N(^nC_4H_9)_4]Cl$ (●) in CH_2F_2 at 20 MPa and 363K. The molar conductivities were obtained by interpolating the data shown in Figures 9 and 10 to the fixed pressure (20 MPa) using polynomial regressions. The lines are merely to guide the eye. The error bars represent the standard uncertainties for Λ, estimated from the experimental uncertainties of the conductivity measurements and the sample concentrations.

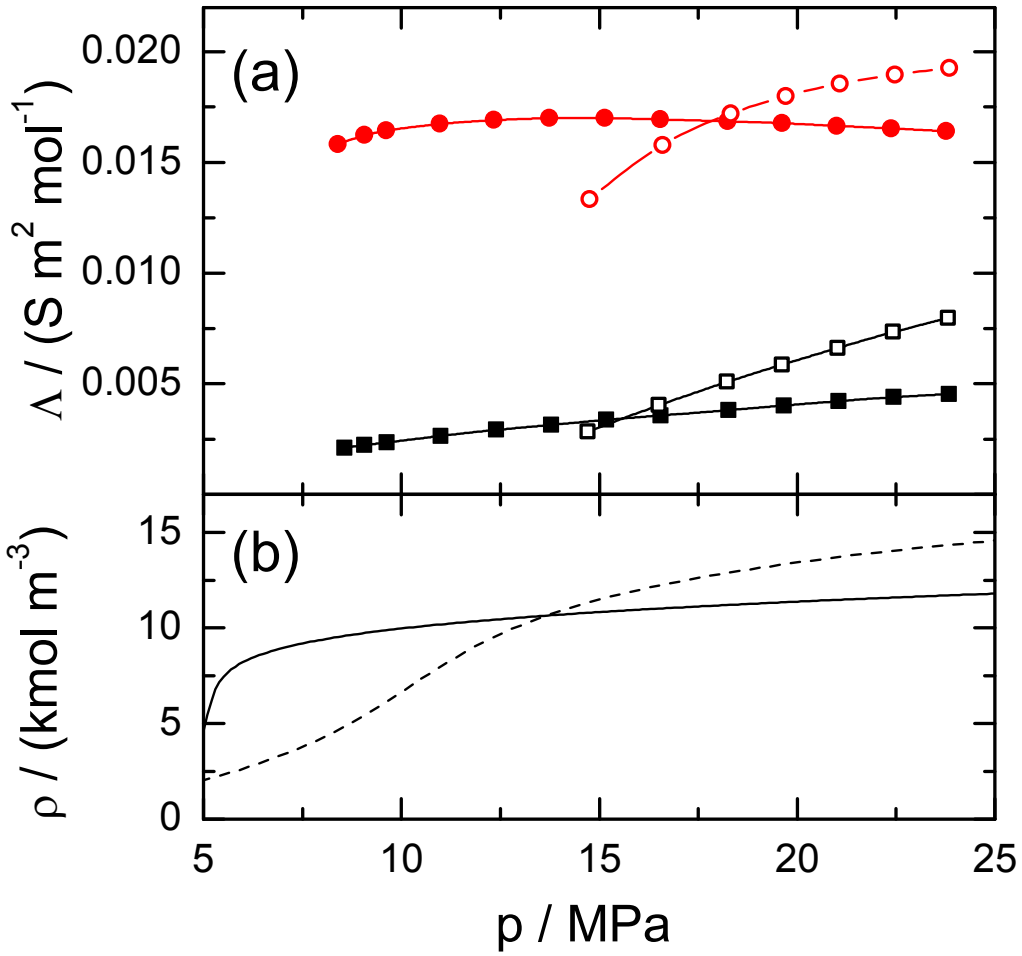

Fig. 12 (a) Molar conductivity (Λ) of $[N(^nC_4H_9)_4][BF_4]$ and $[N(^nC_4H_9)_4]$ $[B\{(3,5\text{-}CF_3)_2C_6H_3\}_4]$ in CHF_2CH_3 and CH_2F_2 at 393.15 K. □, $[N(^nC_4H_9)_4][BF_4]$ in CH_2F_2; ■, $[N(^nC_4H_9)_4][BF_4]$ in CHF_2CH_3; ○, $[N(^nC_4H_9)_4]$ $[B\{(3,5\text{-}CF_3)_2C_6H_3\}_4]$ in CH_2F_2; and ●, $[N(^nC_4H_9)_4]$ $[B\{(3,5\text{-}CF_3)_2C_6H_3\}_4]$ in CHF_2CH_3. The concentration of the electrolyte is ~9 mmol dm^{-3}. (b) The molar density (ρ) plotted as a function of pressure at 393.15 K. The solid and dashed lines represent the isotherms for CHF_2CH_3 and CH_2F_2, respectively.